Acta Materialia 186 (2020) 389–395

Contents lists available at ScienceDirect

Acta Materialia

journal homepage: www.elsevier.com/locate/actamat

Full length article

Sensitivity of twin boundary movement to sample orientation and magnetic field direction in Ni-Mn-Ga

Medha Veligatla[a], Christian Titsch[b], Welf-Guntram Drossel[b,c], Carlos J. Garcia-Cervera[d,e], Peter Müllner[a,*]

[a] Micron School of Materials Science and Engineering, Boise State University, Boise, ID 83725, United States
[b] Institute for Machine Tools and Production Processes, Technische Universität, 09126 Chemnitz, Germany
[c] Fraunhofer Institute for Machine Tools and Forming Technology, 09126 Chemnitz, Germany
[d] Deparment of Mathematics, University of California, Santa Barbara, CA 93117, United States
[e] Basque Center for Applied Mathematics (BCAM), Bizkaia, Spain

ARTICLE INFO

Article History:
Received 19 July 2019
Revised 3 December 2019
Accepted 4 January 2020
Available online 8 January 2020

Keywords:
Ni-Mn-Ga
Micromagnetics
Actuators
Magnetic energy density

ABSTRACT

When applying a magnetic field parallel or perpendicular to the long edge of a parallelepiped Ni-Mn-Ga stick, twin boundaries move instantaneously or gradually through the sample. We evaluate the sample shape dependence on twin boundary motion with a micromagnetics computational study of magnetic domain structures and their energies. Due to the sample shape, the demagnetization factor varies with the direction of the external magnetic field. When the external magnetic field is applied perpendicular to the long edge of the sample, i.e. in the direction in which the demagnetizing field is highest, the magnetic energy intermittently increases when the strength of the applied magnetic field is low. This energy gain hinders the twin boundary motion and results in a gradual switching, i.e. a gradual magnetization reversal as the applied magnetic field is increased. The formation of 180° magnetic domains offsets this effect partially. In contrast, when the applied magnetic field is parallel to the long edge of the sample, i.e. in the direction in which the demagnetizing field is lowest, the energy decreases with each subsequent magnetization domain reversal and the twin boundary moves instantaneously with ongoing switching. The actuation mode with the field parallel to the long sample edge lends itself for on-off actuators whereas the actuation mode with the field perpendicular to the long sample edge lends itself to gradual positioning devices.

1. Introduction

Macroscopic deformation in magnetic shape memory (MSM) alloys occurs when the material is subjected to an external magnetic field or a mechanical stress. Lattice reorientation via twinning in the martensite phase causes this shape change. A MSM single crystal with one twin boundary consists of two twin domains sharing the boundary. These twin domains have different magnetization and crystallographic orientations [1,2]. Depending on the direction of the external magnetic field, one variant grows at the expense of the other as the twin boundary moves along the sample. The maximum magnetic-field-induced strain depends on the martensite structure and lattice parameters and varies between 6% and 12% [2–5] . With a few microseconds response time [6], these materials have great potential as actuators. Numerous research groups have studied the material properties of Ni-Mn-Ga single crystals and its response to variable magnetic fields to improve the performance of MSM actuators [7–14].

In 1995, Ullakko [15] introduced the concept of using magnetic field induced reorientation of martensite variants for magnetically powered actuators. Ullakko suggested that with several percent strain and rapid control, the magnetic shape memory alloys may outperform piezoelectric and magnetostrictive materials. Subsequently, Ullakko et al. demonstrated the deformation in Ni_2MnGa with magnetic fields [16]. In 2004, Suorsa et al. [17] measured various properties that determine the dynamic behavior of a 10 M Ni_2MnGa MSM material. For a sample dimension of 1 mm × 2 mm × 10 mm, the authors reported the acceleration of the sample surface, rise time and actuation velocity to be 5000 m/s^2, 0.2 ms and 1.3 m/s respectively. The switching behavior of the material dictates the response of the actuator. Recently, Saren et al. [6] and Smith et al. [18] reported twin boundary velocities of 39 and 82 m/s implying actuation speeds of 2.4 and 4.8 m/s. Pagounis et al. summarized some recent progress on MSM actuators [19].

The goal of this paper is to study extrinsic factors that influence twin boundary motion in MSM actuators. We apply experimental and numerical methods to Ni-Mn-Ga single crystals in a magnetic field to study the macroscopic response via twin boundary movement and their corresponding mesoscopic magnetic energies. We are particularly

* Corresponding author.
E-mail address: petermullner@boisestate.edu (P. Müllner).

https://doi.org/10.1016/j.actamat.2020.01.011
1359-6454/

interested in the response of the material when exposed to magnetic fields in different directions, namely parallel and perpendicular to the long sample axis. While we performed switching field tests to demonstrate the macroscopic magnetic response, the micromagnetics simulations were carried out to demonstrate the mesoscopic magnetic interactions.

2. Micromagnetics

The field of micromagnetics was pioneered by Brown [20] and a comprehensive review was presented by Chantrell et al. [21]. Many research groups have used micromagnetics to characterize mesoscale magnetic properties of Ni-Mn-Ga alloys [22–29]. The theory of solving the Landau-Lifshitz dynamic equation was applied with various methods such as phase field modeling [23–25,28–30]. This method has been used to study the twin boundary mobility [23], magnetic domain evolutions [30], demagnetization effects [29], and magneto-mechanical properties [24,25] of Ni-Mn-Ga. These research groups studied the magnetic domain evolution as the twin boundary moves along the sample length. In the present study, we simulate the magnetic domain structures for samples with one twin boundary inclined at 45° to the sample edge. For each state, the position of the twin boundary is predetermined and fixed. We do not assess the twin boundary nucleation phase. The magnetic structures start with an initial condition where the sum of magnetization in the *x*, *y*, and *z* direction is unity and evolve to a minimum energy state with respect to time. The position of the twin boundary was determined by the strain on the sample i.e. the fraction $f_{\parallel}$ of region with the *c*-axis (axis of easy magnetization) parallel ($f_{\parallel}$) and perpendicular ($f_{\perp} = 1 - f_{\parallel}$) to the sample length was determined by the strain ε on the sample: $\varepsilon = f_{\perp}(1 - c/a)$, where *a* and *c* are the lattice parameters. Therefore the position of the twin boundary changes with increasing strain on the sample and the *c*-axis across this twin boundary is nearly perpendicular. The location of the twin boundaries are defined fixed by the strain value. Thus we simulate for a static twin boundary contidion at various strains steps that correspond to elongation from 0% to 6% and to compression from 6% to 0% with 0.5% increments. We neglect the twin boundary mobility. This allows us to study the interactions of magnetic domains and twin boundaries in greater detail at equilibrium conditions. Hobza et al. applied a code developed by Garcia-Cervera [31] to study the torque generated by a magnetic field on Ni-Mn-Ga samples with various twin microstructures [22,32]. This code evaluates the actual dynamics (Landau-Lifshitz equation). In our method, we only solve linear systems of equations with constant coefficients. The cost per step of our method is O(*N* log *N*), where *N* is the number of cells. Using this code we obtained magnetic energies for magnetic equilibrium structures that summarize the switching behavior for a single twin boundary system in Ni-Mn-Ga. We map the different energy contributions in the process of magnetic domain evolution. In order to qualitatively compare these energies, the simulations were arranged such that they replicate the experimental setup of a switching field test at small scale. The equilibrium magnetic structures and energies obtained through these simulations take into account the anisotropy, exchange, Zeeman, and stray field energies. The code solves the Landau-Lifshitz-Gilbert equation to approach the minimum energy state:

$$d\mathbf{M}(\mathbf{r})/dt = -\mu_0\gamma\ \mathbf{M}\times\mathbf{H} - \alpha(\mu_0\gamma/M_s)\mathbf{M}\times[\mathbf{M}\times\mathbf{H}] \quad (1)$$

where $\mathbf{M}(\mathbf{r})$ is the magnetization density at position $\mathbf{r}$, γ is the gyromagnetic ratio, α is a dimensionless damping parameter, and $\mathbf{H}$ is the effective local magnetic field vector, which is the negative derivative of total energy with respect to magnetization:

$$\mathbf{H} = -\frac{\delta E}{\mu_0\delta\mathbf{M}} = -(2K_u/\mu_0 M_s^2)(M_2e_2 + M_3e_3)\ + (2C_{ex}/\mu_0 M_s^2)\Delta\mathbf{M} - \nabla\mathbf{U} + \mathbf{H}_{\text{ext}} \quad (2)$$

where K_u is the anisotropy constant, M_s is the saturation magnetization, M_2 and M_3 are magnetization components that are orthogonal to the axis of easy magnetization, e_2 and e_3 are axis directions in which the magnetization is not spontaneous, C_{ex} is the exchange constant, μ_o is magnetic permeability of free space, and $\mathbf{H}_{\text{ext}}$ is the external magnetic field.[1] The individual summation terms in Eq. (2) are the energies associated with magnetocrystalline anisotropy, exchange interaction, stray field, and external applied field (Zeeman energy). In short, the magnetocrystalline energy is the energy associated with the orientation of magnetic domains with respect to the axis of easy magnetization, the exchange energy is the short range interaction energy between neighboring magnetic moments, and the stray field and Zeeman energies are associated with magnetic domain splitting and the external magnetic field respectively. Hobza et al. provide a detailed description of these energy terms and the micromagnetics code [22].

3. Experiments and simulations

All the experiments were conducted on a Ni-Mn-Ga single crystal with 10 M martensite structure and composition $Ni_{49.5}Mn_{28.8}Ga_{21.7}$ (Goodfellow). A rectangular sample with dimensions 3.93 mm × 2.86 mm × 1.06 mm was cut with all faces parallel to {1 0 0}. X-ray diffraction and energy dispersive X-ray spectroscopy were done with a Bruker D8 Discover diffractometer and a Hitachi S-3400N-II scanning electron microscope equipped with an Oxford Instruments Energy EDS to confirm the crystal structure and the composition. Magnetic switching field experiments were conducted with a ADE model 10 vibrating sample magnetometer (VSM). For the VSM experiments, the sample was mounted to a quartz tube and exposed to an increasing magnetic field. The experiments were done with two configurations, such that the magnetic field was parallel to the longest (designated “parallel”) and the intermediate (designated “perpendicular”) edge of the sample. First the sample was placed in the field with parallel sample configuration. The field was increased from 0 to 1.2 T to fully saturate the sample and then reduced to 0 T. Then, the electromagnet was rotated such that the sample was in perpendicular configuration. In this setup the field was increased from 0 to 1.2 T and reduced to 0 T. Then the magnet orientation was rotated back to the parallel configuration. We conducted 6 experiments with alternating parallel and perpendicular configurations and measured the magnetization as a function of magnetic field strength. At the beginning of the experiments in parallel and perpendicular configurations, the sample starts with fully extended (6% strain) and fully compressed (0% strain) states, respectively.

We conducted micromagnetics simulations to assess the equilibrium magnetic structure and to calculate the magnetic energies of Ni-Mn-Ga samples for magnetic fields in parallel and perpendicular configuration and for various deformation states. The strain was varied from fully compressed state (i.e. 0%) to fully elongated state (i.e. 6%) in increments of 0.5%. The sample dimensions used for simulating 0% and 6% correspond to 1.55 μm × 0.53 μm × 0.36 μm ($L \times W \times t$) and 1.64 μm × 0.50 μm × 0.36 μm ($L \times W \times t$). The length (L) and width (W) of the sample were varied with respect to the strain while the thickness (t) was kept constant. The sample dimensions corresponding to each strain are given in Table 1 in the Appendix. A twin boundary at 45° to the sample edge was introduced when the strain was varied from 0.5% to 5.5%. The position of the twin boundary was determined by the strain on the sample i.e. the fraction of region with the *c*-axis (axis of easy magnetization) parallel and perpendicular to the sample length was determined by the strain on the sample (APPENDIX A, Table 1). The entire simulation had 73,728 cells defined such that 384 were along the longest sample dimension and 192

[1] Eqs. (1) and (2) are given in SI unites and differ from those given in Ref. [31].

were along the intermediate dimension. Thus at 3% strain, each cell size along the long and intermediate dimensions were 4.17 nm and 2.70 nm respectively. Each simulation ran for 20,000 iterations. To obtain a magnetic structure with minimum energy configuration, we added multiple runs that continued from the previously ended run. In total, we did 380,000 iterations for each simulation condition to obtain the minimum energy state. Since the experimental results (Fig. 2) show the occurrence of switching for parallel and perpendicular configurations around 225 mT and 375 mT respectively, the simulations were also conducted at such low magnetic field values. Upon increasing the field to 300 mT, we found that the simulation results explained the experimental results sufficiently (as outlined in the discussion) such that we terminated the computational study. Therefore, simulations were conducted at 100 mT, 150 mT, 200 mT, 250 mT, and 300 mT for all strain values. The direction of the magnetic field was applied parallel and perpendicular to the longest dimension of the sample (Fig. 1). Fig. 1(a) and (b) illustrates the initial sample size and the direction of the magnetic field for perpendicular (fully compressed to 0% strain) and parallel (fully elongated to 6% strain) sample configurations. The lines inside these rectangular schematics marked as 'c' represent the orientation of the axis of easy magnetization in their fully compressed and elongated states.

4. Results

Results of the VSM switching field experiments in parallel and perpendicular sample configuration are shown in Fig. 2. The plot is a record of magnetization vs. external magnetic field $\mu_0 H$. For the sample setup with parallel configuration, the magnetization increased linearly until 0.4 T, followed by a sudden rise to near saturation. The quick and complete rise indicates that twinning occurred throughout the entire sample. (This event is often referred to as switching.) For the sample setup with perpendicular configuration the increase in magnetization up to saturation occurred gradually over multiple small steps from 0.25 T to 0.38 T.

Fig. 3 is a plot of numerically calculated magnetic energy densities with respect to sample deformation at various magnetic fields for the parallel configuration. In this setup since we started the experiment with a fully elongated sample, the deformation started at 6% and proceeded to 0% and the energy density decreased monotonically with deformation. With increasing magnetic field, the slope magnitude increased.

Fig. 4 is a plot showing the numerically calculated magnetic energy densities with sample deformation at various magnetic fields for the perpendicular configuration, starting from the fully compressed state (i.e. 0% strain). The strain on the abscissa goes from 0% to 6%. At 100 mT, with increasing strain, the energy density decreased initially, went through a local minimum, then increased and went through a local maximum before it decreased again. At 150 mT, with increasing strain, the energies decreased with a steeper slope compared to when the field was at 100 mT. Then the slope flattened with increasing strain and went through a subtle minimum at 5% strain and a subtle maximum at 5.5% strain. We call this localized increase in energy during elongation as local maxima. Following the local maxima, the energy again decreased. Therefore, the local energy maximum was between 4.5% and 5% strain for 100 mT and at 5.5% strain for 150 mT. At magnetic fields equal to or larger than 200 mT, the energy density decreased monotonically with increasing strain. The slope of the energy got steeper with increasing magnetic field. We obtained energy plots for all simulated states, which were 130 (13 strain states, 2 field directions, and 5 field values). In the following, we selected all 13 strain states for the lowest (100 mT) and highest (300 mT) magnetic field values to display the magnetic domain structures (Fig. 5). From these states, we selected the states with 100 mT in parallel configuration, fully compressed (0% strain, Fig. 6) and fully expanded (6% strain, Fig. 7) and with 100 mT in perpendicular (Fig. 8) and parallel (Fig. 9) configuration at 4.5% strain to highlight the impact of field direction on magnetic energy distributions.

Fig. 5(a) and (b) are the equilibrium magnetic domain structures obtained for parallel sample configuration. Fig. 5(a) and (b) show the magnetic structure evolution for a single twin boundary system starting from 6% to 0% at 100 mT and 300 mT respectively. In both cases, one twin domain had a single magnetic domain structure (represented in red, magnetic moments pointing to the left) while the other twin domain across the twin boundary had multiple magnetic 180° domains (yellow, magnetic moments pointing up, and green, magnetic moments pointing down). The magnetic domain boundaries within the right twin were 180° domain boundaries. The twin boundary carried 90° magnetic domain boundaries where the yellow/red boundary was a head-to-tail boundary and the green/red domain

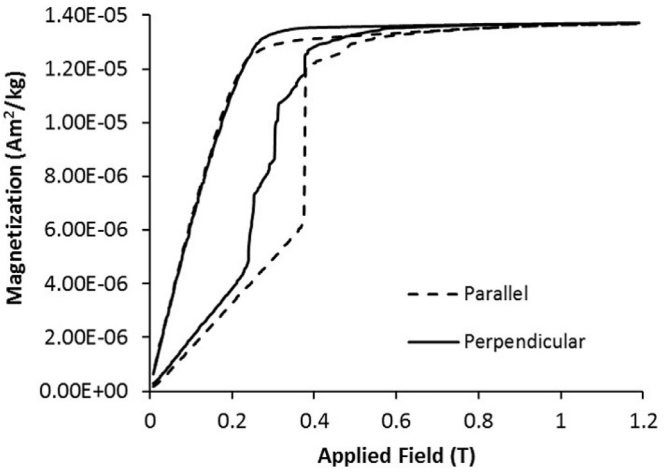

Fig. 2. Switching behavior of $Ni_{49.5}Mn_{28.8}Ga_{21.7}$. The curves represent the change in magnetization as a function of applied magnetic field for magnetic fields applied in different directions. The dotted and solid curves correspond to perpendicular and parallel sample configurations.

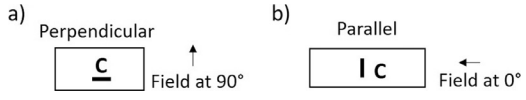

Fig. 1. Schematics of samples used for micromagnetics simulations and experimental set up with respect to magnetic field. The arrows indicate the direction of magnetic field. (a) Initial sample dimension for perpendicular sample configuration: starting with fully compressed (0% strain) sample and (b) initial sample dimension for parallel configuration: starting with fully elongated (6% strain).

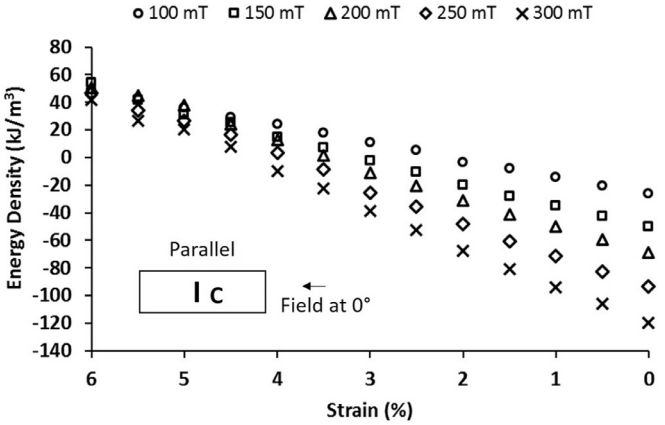

Fig. 3. Numerical calculation of magnetic energy densities as a function of strain in parallel sample configuration. The energy densities are plotted against sample deformation as they occur during an experiment (i.e. starting from fully elongated to fully compressed). The inset shows a sample with the direction of easy magnetization (represented by c) and the orientation of the external magnetic field.

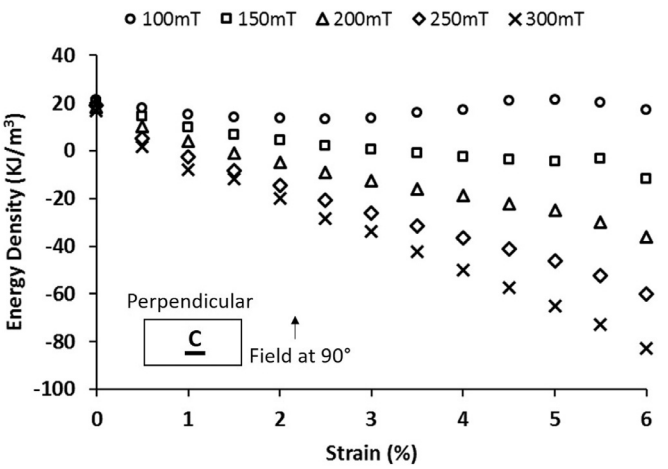

Fig. 4. Numerical calculation of magnetic energy densities as a function of strain in perpendicular sample configuration. The energy densities are plotted against sample deformation as they occur during an experiment (i.e. starting from fully compressed to fully elongated). The figure inset shows a sample with the direction of easy magnetization (represented by c) and the orientation of the external magnetic field.

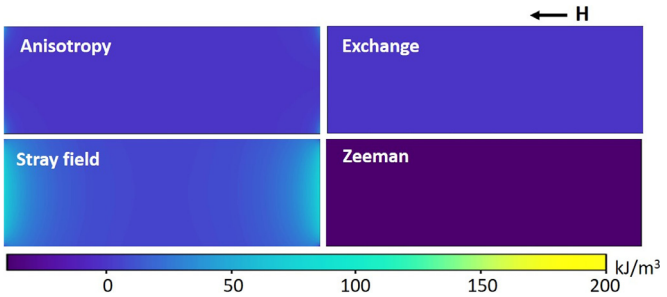

Fig. 6. Energy maps at 0% strain in a 100 mT magnetic field for sample setup in parallel configuration. The direction of the magnetic field is indicated by the arrow. Each plot as labeled represents the anisotropy, exchange, stray field, and Zeeman energy associated with the magnetic domain structure at equilibrium. The maps are homogeneous because the sample has no twin and magnetic domain boundaries.

boundary was a tail-to-tail boundary. Fig. 5(c) and (d) are the equilibrium magnetic structures obtained for perpendicular sample configuration. Fig. 5(d) shows the magnetic domain structure evolution for a single twin boundary system from 0% to 6% strain at 300 mT. It is similar to Fig. 5(a) and (b) where one variant had a single domain structure and the other variant across the twin boundary had multiple magnetic domains. In this case, however, the left twin domain with the axis of easy magnetization horizontal had multiple magnetic domains. These results agree with the experimental characterization of magnetization reported by Faran et al. [33]. Whereas at 100 mT (Fig. 5(c)) as the magnetic structure evolution occurred from 0% to 6% strain, both twin domains contained multiple magnetic domains. Up to a strain of 3.5%, the left twin domain contained one blue magnetic domain (magnetic moments pointing to the right) and the right twin

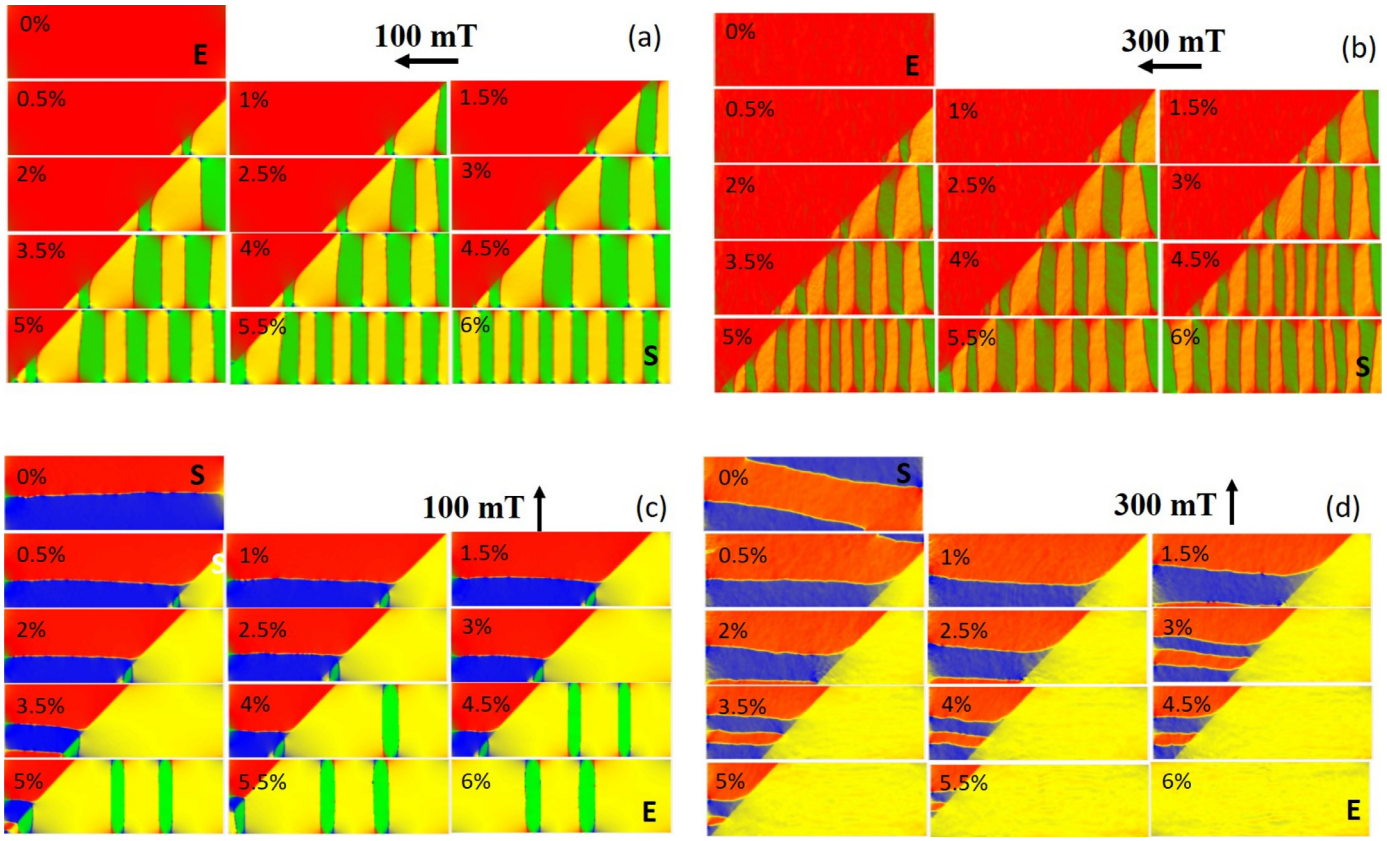

Fig. 5. Evolution of the magnetic domain structure obtained from simulations for a switching field test at 100 and 300 mT in a single twin boundary state. (a) and (b) are the equilibrium domain structures for parallel sample configuration and (c, d) are the equilibrium domain structures for perpendicular sample configuration. The letter "S" and "E" indicate the start and end of deformation as the switching field test is performed i.e. the sample deforms from 6% to 0% for parallel and 0% to 6% for perpendicular sample configuration. The colors here indicate the direction of magnetization in the magnetic domains: red (←), blue (→), yellow (↑), and green (↓). The red hue in the yellow magnetic domains in (b) is due to a significant rotation of magnetic moments towards the left and away from the direction of easy magnetization as a result of higher magnitude of magnetic field (300 mT). (For interpretation of the references to colour in this figure legend, the reader is referred to the web version of this article.)

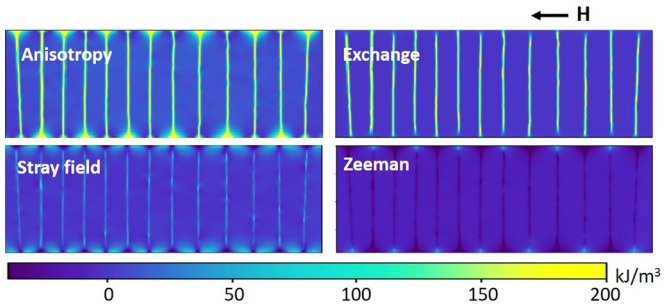

Fig. 7. Energy maps at 6% strain in a 100 mT magnetic field for sample setup in parallel configuration. High densities of anisotropy and exchange energy decorate the magnetic domain boundaries.

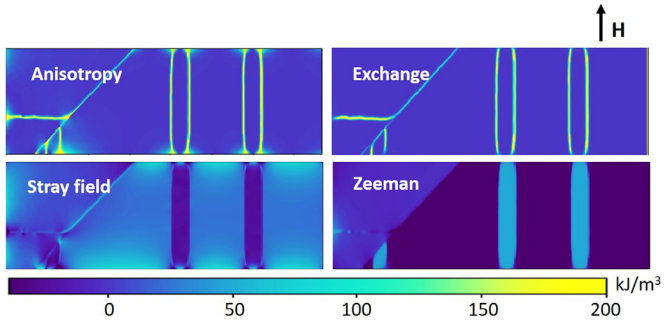

Fig. 8. Energy maps at 4.5% strain in a 100 mT magnetic field for sample setup in perpendicular configuration. The twin boundary has lower energy than the magnetic domain boundaries. The vertical magnetic domains with magnetization pointing down (green in Fig. 5) have low stray field and high Zeeman energy.

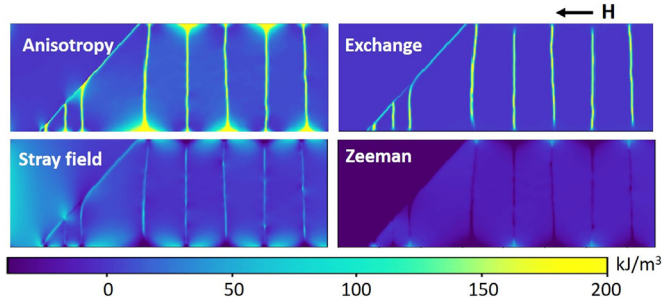

Fig. 9. Energy maps at 4.5% strain in a 100 mT magnetic field for sample setup in parallel configuration. The twin domain with *c* parallel to the longest edge (red in Fig. 5) has low Zeeman energy.

domain had one green magnetic domain (magnetic moments pointing down). The blue and green magnetic domains met at the twin boundary in head-to-tail configuration. From 4% to 6% strain, additional green magnetic domains formed in the right twin domain. These green magnetic domains extended across the entire sample.

The four energy terms (anisotropy, exchange, stray field, and Zeeman) that are associated with the total magnetic energy calculation are shown for selected cases in Figs. 6–9. Figs. 6 and 7 demonstrate the energies corresponding to 0% and 6% strain respectively at 100 mT for parallel sample configuration. Since there were no magnetic domain boundaries for the 0% strain case (see Fig. 5(a)) all the energies were uniformly distributed across the sample (Fig. 6). In the case of 6% strain, since there were multiple magnetic domains (see Fig. 5(a)), the anisotropy and exchange energy was high at magnetic domain boundaries compared to the regions within the domains (Fig. 7). Figs. 8 and 9 show the energies associated with 4.5% strain at 100 mT for perpendicular and parallel configuration respectively. In Fig. 8, at the twin boundary and magnetic domain boundaries (where the domain orientation changes due to the transition) the anisotropy and exchange energies are high compared to the regions that have a uniform orientation of magnetic moments. The stray field energy was quite uniform across the sample but the alternating domain regions (light blue in Fig. 8 bottom right, green in Fig. 5) which had the magnetic moments pointing in the direction opposite to the external field had significantly heightened Zeeman energy and lowered stray field energy. Fig. 9 represents the same strain state (4.5%, 100 mT) in parallel configuration. While the anisotropy, exchange and stray field energies were high at transition regions compared to the regions with uniform orientation of magnetic moments, the Zeeman energy on the whole fell on the lower end of the energy scale with no distinguished change in energy from one magnetic domain to another.

Fig. 10(a) and (b) shows the contribution from each energy term (anisotropy, exchange, stray field and Zeeman energy) towards the total magnetic energy for different strain states at 100 mT in parallel and perpendicular configurations. From comparing the energies in Fig. 10 with the magnetic domain evolution in Fig. 5 follows that the anisotropy and exchange energies increased with increasing number of magnetic domains in the structure whereas the stray field and Zeeman energies decreased. For the perpendicular field configuration (Fig. 10(b)), at 4% strain and 4.5% strain the Zeeman energy increased while the stray field energy decreased.

5. Discussion

Here we qualitatively compare the experimental and numerical results. We do not attempt to compare the experimental and numerical results quantitatively because the volume of the simulated sample is orders of magnitude smaller than that of the experimental sample. Experimental data (Fig. 2) shows that for parallel sample configuration switching in the material is abrupt whereas for perpendicular sample configuration it occurs gradually in a step like behavior. Results from numerical calculations for parallel sample configuration show that the magnetic energy density monotonously decreases with increasing magnetic field and strain (Fig. 3). This decrease in energy density explains the spontaneous switching that we see in the experimental data. Once the magnetic field provides enough driving force to nucleate a twin boundary, the twin boundary moves through the entire sample since the energy continuously decreases as the twin boundary advances. In the case of perpendicular sample configuration (Fig. 4), results from numerical calculations at 100 mT show a localized increase in energy from 4% to 5.5% strain. With increasing magnetic field, the overall energy becomes lower and so does the local energy maximum at large strain. Above 200 mT magnetic field, the total energy follows the same monotonously decreasing trend as for the parallel configuration. This means that when a twin boundary forms at low magnetic field strength, it can advance only as long as the energy decreases and stops at a strain where the energy is a local minimum. To overcome the energy barrier (i.e. the local maximum) the magnetic field must increase. Since the material remains at the energy valley until the required magnetic field is applied, the twin boundary movement is retarded. This results in gradual, step-like switching.

The shape of the sample plays an important role for the twin boundary motion. The motion of the twin boundary magnetizes the sample and, thus, reduces the Zeeman energy. This is the main driving force for twin domain switching. As the sample gets magnetized, the stray field energy increases. For a parallelepiped bar (present study), in the perpendicular configuration, the magnetic field is perpendicular to the long axis of the sample, which results in a higher demagnetization factor (and, thus, higher stray field energy) compared to the parallel configuration (where the field is parallel to the long axis of the sample). This effect is shown in Fig. 10 where the stray field energy increases strongly with increasing strain between

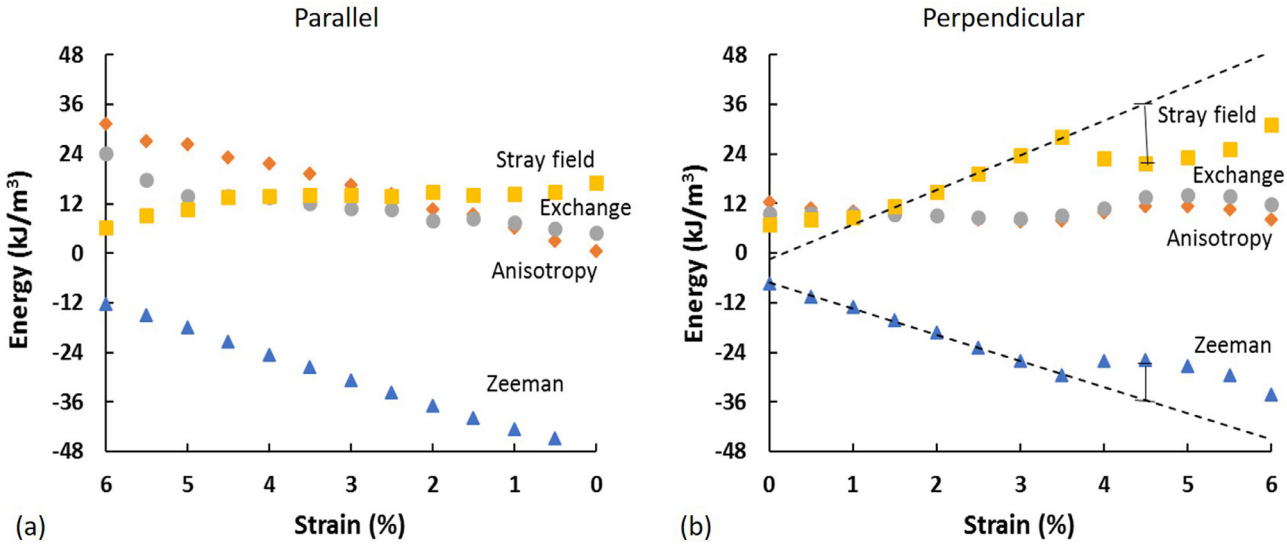

Fig. 10. Contributions from anisotropy, exchange, stray field and Zeeman energies to the total magnetic energy of equilibrium magnetic structures obtained at different strain states at 100 mT. (a) In parallel configuration and (b) in perpendicular configuration.

1% and 3.5% strain for the perpendicular configuration (Fig. 10(b)). In contrast, the stray field energy increases only moderately with ongoing deformation in the parallel configuration (Fig. 10(a)).

To lower the stray field energy the magnetic structure tends to form multiple domains separated by 180° domain walls. This happens for perpendicular and parallel sample configurations (Fig. 5). However, in parallel configuration, 180° magnetic domains form only in that twin domain where the axis of easy magnetization is perpendicular to the magnetic field. In this case, the 180° magnetic domains reduce the stray field energy without changing the Zeeman energy. In contrast, because of the large demagnetization factor perpendicular to the longest edge of the sample, 180° magnetic domains form in both twin domains for the perpendicular configuration. This means that in the twin domain with the easy axis of magnetization parallel to the magnetic field, the green domains (in Fig. 5(c)) are magnetized opposite to the direction of the magnetic field. These domains increase the Zeeman energy. The increase in Zeeman energy partially compensates for the decrease in stray field energy. This can be explained by comparing the domain structures in Fig. 5(a) (100 mT, parallel configuration) and Fig. 5(c) (100 mT, perpendicular configuration). In Fig. 5(a), as the material is magnetized parallel to the length of the sample, the demagnetization factor is less than the perpendicular field case shown in Fig. 5(c). Due to this large demagnetization for case 5c, the stray field energy is lowered at the expense of Zeeman energy (Fig. 10). This lowering of stray field energy results in domain splitting for case 5c, while case 5a contains a single red domain.

These results have implications for the design of magnetic shape memory alloy actuators. If one attempts to build an on-off actuator, i. e. a device that switches abruptly between two states, the magnetic field must be applied parallel to the long direction of the magnetic shape memory element. In this configuration, the device switches instantaneously from fully elongated to fully contracted. To switch abruptly from fully contracted to fully extended requires a strong magnetic pulse perpendicular to the sample where the field strength of the pulse is sufficient to saturate the sample. If one attempts to build a positioning actuator capable of adjusting a position gradually, the magnetic shape memory element must be long and the magnetic field must be applied perpendicular to the stroke. Gradual resetting with a magnetic field parallel to the direction of the stroke is not possible since such actuation results in instantaneous and complete switching. Instead, resetting can be achieved with second actuator in "push-push" configuration [34].

6. Conclusions

We combined experiments and numerical calculations to study the effect of magnetic field to sample orientation on twin boundary motion with varying magnetic fields on a rectangular bar sample. Lowering the Zeeman energy is the main driving force for twin domain switching. As the twin boundary moves through the sample, the sample gets magnetized, which increases the stray field energy. This effect is stronger when the magnetic field is perpendicular to the longest sample extension because of a higher demagnetization factor. The demagnetizing field hinders twin domain switching in the perpendicular configuration. The formation of 180° magnetic domains partially offsets this shape effect. The perpendicular configuration lends itself for a gradual positioning device while the parallel configuration is ideal for an on-off switch.

Acknowledgments

We thank Andrew Armstrong for assisting with the experimental set-up. PM acknowledges partial financial support from the National Science Foundation through project DMR-1710640 and the high-performance R2 compute cluster (DOI: 10.18122/B2S41H) provided by Boise State University's Research Computing Department.

APPENDIX A

See Table 1.

Table 1
Simulated sample sizes and twin fractions corresponding to strain.

Strain (%)	Length (μm)	Width (μm)	Twin fraction (f_t)
0	1.55	0.517	1
0.5	1.56	0.533	0.91
1	1.568	0.530	0.83
1.5	1.57	0.528	0.75
2	1.58	0.525	0.67
2.5	1.59	0.522	0.58
3	1.60	0.52	0.5
3.5	1.60	0.517	0.41
4	1.61	0.514	0.33
4.5	1.62	0.511	0.25
5	1.63	0.509	0.17
5.5	1.63	0.506	0.08
6	1.64	0.503	0

References

[1] R. Tickle, R.D. James, T. Shield, M. Wuttig, V.V. Kokorin, Ferromagnetic shape memory in the NiMnGa system, IEEE Trans. Magn. 35 (1999) 4301–4310, doi: 10.1109/20.799080.

[2] K. Ullakko, J.K. Huang, C. Kantner, R.C. O'Handley, V.V. Kokorin, Large magnetic-field-induced strains in Ni_2MnGa single crystals, Appl. Phys. Lett. 69 (1996) 1966–1968, doi: 10.1063/1.117637.

[3] S.J. Murray, M. Marioni, S.M. Allen, R.C. O'Handley, T.A. Lograsso, 6% magnetic-field-induced strain by twin-boundary motion in ferromagnetic Ni-Mn-Ga, Appl. Phys. Lett. 77 (2000) 886–888, doi: 10.1063/1.1306635.

[4] A. Sozinov, N. Lanska, A. Soroka, W. Zou, 12% magnetic field-induced strain in Ni-Mn-Ga -based non-modulated martensite, Appl. Phys. Lett. 102 (2013) 021902 1-5, doi: 10.1063/1.4775677.

[5] O. Söderberg, Y. Ge, A. Sozinov, S.P. Hannula, V.K. Lindroos, Recent breakthrough development of the magnetic shape memory effect in Ni-Mn-Ga alloys, Smart Mater. Struct. 14 (2005) S223–S235, doi: 10.1088/0964-1726/14/5/009.

[6] A. Saren, T. Nicholls, J. Tellinen, K. Ullakko, Direct observation of fast-moving twin boundaries in magnetic shape memory alloy Ni-Mn-Ga 5M martensite, Scr. Mater. 123 (2016) 9–12, doi: 10.1016/j.scriptamat.2016.04.004.

[7] Y.W. Lai, R. Schäfer, L. Schultz, J. McCord, Direct observation of ac field-induced twin-boundary dynamics in bulk NiMnGa, Acta Mater 56 (2008) 5130–5137, doi: 10.1016/j.actamat.2008.06.030.

[8] E. Pagounis, R. Chulist, M.J. Szczerba, M. Laufenberg, High-temperature magnetic shape memory actuation in a Ni-Mn-Ga single crystal, Scr. Mater. 83 (2014) 29–32, doi: 10.1016/j.scriptamat.2014.04.001.

[9] L. Sturz, A. Drevermann, U. Hecht, E. Pagounis, M. Laufenberg, Production and characterization of large single crystals made of ferromagnetic shape memory alloys Ni-Mn-Ga, Phys. Procedia 10 (2010) 81–86, doi: 10.1016/j.phpro.2010.11.079.

[10] D.C. Dunand, P. Müllner, Size effects on magnetic actuation in Ni-Mn-Ga shape-memory alloys, Adv. Mater. 23 (2011) 216–232, doi: 10.1002/adma.201002753.

[11] S.A. Wilson, R.P.J. Jourdain, Q. Zhang, R.A. Dorey, C.R. Bowen, M. Willander, et al., New materials for micro-scale sensors and actuators, Mater. Sci. Eng. R: Rep. 56 (2007) 1–129, doi: 10.1016/j.mser.2007.03.001.

[12] B. Holz, H. Janchoa, L. Ricardi, Compact MSM Actuators - concept for highest force exploitation, in: H Borgmann (Ed.), Proc. ACTUATOR 2012, 13th Int. Conf. on New Actuators, Messe Bremen, Bremen, Germany, 2012, pp. 663–666.

[13] N. Gabdullin, S.H. Khan, Review of properties of magnetic shape memory (MSM) alloys and MSM actuator designs, J. Phys. Conf. Ser. 588 (2015) 012052 1–5, doi: 10.1088/1742-6596/588/1/012052.

[14] M. Kohl, M. Gueltig, V. Pinneker, R. Yin, F. Wendler, B. Krevet, Magnetic shape memory microactuators, Micromachines (Basel) 5 (2014) 1135–1160, doi: 10.3390/mi5041135.

[15] K. Ullakko, Magnetically controlled shape memory alloys: a new class of actuator materials, J. Mater. Eng. Perform. 5 (1996) 405–409, doi: 10.1007/BF02649344.

[16] K. Ullakko, J.K. Huang, V.V. Kokorin, R.C. O'Handley, Magnetically controlled shape memory effect in Ni_2MnGa intermetallics, Scr. Mater. 36 (1997) 1133–1138, doi: 10.1016/S1359-6462(96)00483-6.

[17] I. Suorsa, E. Pagounis, K. Ullakko, Magnetic shape memory actuator performance, J. Magn. Magn. Mater. 272–276 (2004) 2029–2030, doi: 10.1016/j.jmmm.2003.12.1026.

[18] A.R. Smith, J. Tellinen, K. Ullakko, Rapid actuation and response of Ni-Mn-Ga to magnetic-field-induced stress, Acta Mater. 80 (2014) 373–379, doi: 10.1016/j.actamat.2014.06.054.

[19] E. Pagounis, P. Müllner, Materials and actuator solutions for advanced magnetic shape memory devices (review), Oral Contributions B3 Magnetostrictive/MSM Actuators, Technical papers, 2018, pp. 205–211.

[20] W.F. Brown, Domains, micromagnetics, and beyond: reminiscences and assessments, J. Appl. Phys. 49 (1978) 1937–1942, doi: 10.1063/1.324811.

[21] W. Chantrell, M. Wongsam, T. Schrefl, J. Fidler, Micromagnetics I: basic principles, Encycl. Mater. Sci. Technol. (2001) 5642–5650, doi: 10.1016/b0-08-043152-6/00984-0.

[22] A. Hobza, P. Müllner, Magnetic torque in single crystal Ni-Mn-Ga, Shape Mem. Superelast. 3 (2017) 139–148, doi: 10.1007/s40830-017-0106-3.

[23] Y.M. Jin, Effects of twin boundary mobility on domain microstructure evolution in magnetic shape memory alloys: phase field simulation, Appl. Phys. Lett. 94 (2009) 062508 1–3, doi: 10.1063/1.3081011.

[24] Q. Peng, Y.J. He, Z. Moumni, A phase-field model on the hysteretic magneto-mechanical behaviors of ferromagnetic shape memory alloy, Acta Mater. 88 (2015) 13–24, doi: 10.1016/j.actamat.2015.01.044.

[25] Q. Peng, Q. Sun, M. Chen, Phase- field simulations of partial pseudoelastic stress-strain behavior and microstructure evolution of Ni-Mn-Ga, Mater. Sci. Eng. A 669 (2016) 428–436, doi: 10.1016/j.msea.2016.05.099.

[26] Y.M. Jin, Y.U. Wang, A. Kazaryan, Y. Wang, D.E. Laughlin, A.G. Khachaturyan, Magnetic structure and hysteresis in hard magnetic nanocrystalline film: computer simulation, J. Appl. Phys. 92 (2002) 6172–6181, doi: 10.1063/1.1510955.

[27] H.B. Huang, X.Q. Ma, J.J. Wang, Z.H. Liu, W.Q. He, L.Q. Chen, A phase-field model of phase transitions and domain structures of NiCoMnIn metamagnetic alloys, Acta Mater. 83 (2015) 333–340, doi: 10.1016/j.actamat.2014.10.014.

[28] J.X. Zhang, L.Q. Chen, Phase-field model for ferromagnetic shape-memory alloys, Philos. Mag. Lett. 85 (2005) 533–541, doi: 10.1080/09500830500385527.

[29] Q. Peng, J. Huang, M. Chen, Effects of demagnetization on magnetic-field-induced strain and microstructural evolution in Ni-Mn-Ga ferromagnetic shape memory alloy by phase- field simulations, Mater. Design 107 (2016) 361–370, doi: 10.1016/j.matdes.2016.06.050.

[30] Y.M. Jin, Effects of magnetostatic interaction on domain microstructure evolution in magnetic shape memory alloys : phase field simulation, Philos. Mag. 90 (1–4) (2010) 169–176, doi: 10.1080/14786430902758671.

[31] C.J. Garcia-Cervera, Numerical micromagnetics : a review, Bol. Soc. Esp. Mat. Apl. (2007) 1–33.

[32] A. Hobza, C.J. García-Cervera, P. Müllner, Twin-enhanced magnetic torque, J. Magn. Magn. Mater. 458 (2018) 183–192, doi: 10.1016/j.jmmm.2018.03.014.

[33] E. Faran, I. Benichou, S. Givli, D. Shilo, The effects of magnetic and mechanical microstructures on the twinning stress in Ni-Mn-Ga, J. Appl. Phys. 118 (2015) 244104 1–9, doi: 10.1063/1.4939179.

[34] A.R. Kathrin Schlüter, B. Holz, Principle design of actuators driven by magnetic shape memory alloys, Adv. Eng. Mater. 14 (2012) 682–686 https://doi.org/10.1002/adem.201200078 .